Transition rates for a $S \geq 1$ model coupled to a phonon bath

Kyungwha Park*
Department of Physics, Virginia Polytechnic Institute and State University, Blacksburg, Virginia 24061
(Dated: February 1, 2008)

We investigate transition rates between different spin configurations for $S \geq 1$ spins weakly coupled to a d-dimensional phonon bath. This study is motivated by understanding observed magnetization relaxation as a function of temperature in diverse magnetic systems such as arrays of magnetic nanoparticles and magnetic molecules. We assume that the magnetization of the spin system relaxes through consecutive emission or absorption of a single phonon. From a weak, linear spin-phonon coupling Hamiltonian, we derive transition rates that would be used to examine dynamic properties of the system in kinetic Monte Carlo simulations. Although the derived phonon-assisted transition rates satisfy detailed balance, in the case of two and three dimensional phonon baths, transitions between degenerate states are not allowed. Thus, if there are no alternative paths along which the spin system can relax, the relaxation time diverges. Otherwise, the system finds other paths, which leads to an increase in the relaxation time and energy barrier. However, when higher-order phonon processes are included in the transition rates, it is found that the system can reach the states which were inaccessible due to the forbidden transitions. As a result, the system recovers some of the dynamic properties obtained using the Glauber transition rate.

PACS numbers: 75.60.Jk,02.70.Tt,61.20.Lc

I. INTRODUCTION

In many physical and chemical nanoscale systems ranging from semiconductor quantum dots to arrays of magnetic nanoparticles or nanoscale magnetic molecules, dynamic properties play a crucial role in understanding the underlying physics and in designing systems of interest for practical applications. For example, the time evolution of quantum systems into decoherence needs to be fully understood in various local environments in order to build scalable quantum computers. It is also important to investigate the spin-lattice relaxation time T_1 and the magnetization relaxation time for recently synthesized nanoscale magnetic systems to use them as information storage devices.

To study the dynamic properties of the systems discussed above, it is common to consider interactions of the systems with their environment. The environment is typically described as a heat bath, which has a much shorter relaxation time than the systems. Depending on the physical quantities to be calculated, one has to choose an appropriate bath. To understand decoherence mechanisms in quantum dots at low temperatures, one often considers an interaction between electron spins and a spin bath consisting of a large number of $S = 1/2$ spins that mimic nuclear spins.[1,2] To estimate the spin-lattice relaxation time in quantum dots, one should take into account electronic spins coupled to a phonon bath.[3] In nanoscale magnetic systems such as arrays of magnetic nanoparticles,[4,5] single-molecule magnets,[6,7,8] and single-chain magnets,[9,10,11] the effect of nuclear spins is minimal, so a phonon bath becomes more relevant than a spin bath. For a single-molecule magnet embedded in a three-dimensional lattice, transition rates between different spin configurations have been derived from coupling to the lattice via magneto-elastic coupling.[6,7,8,12] The magnetization relaxation time was estimated using these transition rates and quantum tunneling rates, being in good agreement with experimental data.[7] For a nearest-neighbor interacting ferromagnetic Ising system, transition rates were derived from a weak, linear coupling of the system to a one-, two-, or three-dimensional phonon bath.[13,14,15] Using these phonon-assisted transition rates, kinetic Monte Carlo simulations were performed to measure the lifetime of the metastable state or magnetization relaxation time at low temperatures. The Monte Carlo simulations revealed that the dynamic properties obtained using the phonon-assisted transition rates greatly differ from those using other transition rates, such as Glauber[16] or Metropolis.[17] It is known that the Glauber transition rate can be derived from a coupling of a spin system to a fermionic bath.[18] Recently, it was shown that the soft Glauber transition rate[19] requires different interpretation in the form of the lifetime of the metastable state at low temperatures, although the energy barrier to reach equilibrium is the same as that for the standard hard Glauber transition rate.[20] Therefore, selection of a proper bath and relevant transition rates is critical in understanding dynamic properties. The transition rates derived by Park *et al.*[13,14,15] (two- and three-dimensional baths) and other groups[7,8,21] (three-dimensional bath) using coupling to a phonon bath, share a common feature that the rates become zero for degenerate states. Very recently, the derived phonon-assisted transition rates were used to examine the nanostructure of field-driven solid-on-solid interfaces.[22] It was found that the phonon-assisted rates provide significant differences from other types of transition rates, such as the Glauber dynamics.

In this study, targeting arrays of weakly interacting magnetic nanoparticles, single-molecule magnets, and single-chain magnets, we generalize the formalism used

for an Ising system in Refs.13,14,15 to a $S \geq 1$ model on a lattice. Each spin in the model interacts via its nearest neighbors and has easy-axis single-ion anisotropy. We assume that all spins in the model are weakly coupled to a phonon bath in $d = 1, 2$, or 3 dimensions. Considering that spin relaxation occurs through first-order one-phonon emission or absorption processes, we derive transition rates for one-, two-, and three-dimensional phonon baths. In the cases of $d = 2$ and 3, some transitions or relaxation paths are inaccessible because transition rates between degenerate states vanish. This results in increasing magnetization relaxation time and energy barrier to be overcome. However, when higher-order phonon processes are included, other relaxation paths are opened up, leading to shortening of the relaxation time compared to the first-order phonon processes. The formalism for the phonon-assisted transition rates is presented in Sec.II. The consequences of using the derived transition rates are discussed in the context of kinetic Monte Carlo simulations in Sec.III. Higher-order processes and their effects on dynamic properties are presented in Sec.IV. The conclusion follows in Sec.V.

II. FORMALISM FOR PHONON-ASSISTED TRANSITION RATES

Although the current formalism can be applied to more general cases, we start with the following Hamiltonian for N_s spins ($S \geq 1$) on a lattice.

$$\mathcal{H}_{\rm sp} \;=\; -J \sum_{\langle i,j \rangle} S_i^z S_j^z - D \sum_{i=1}^{N_s} (S_i^z)^2 - H \sum_{i=1}^{N_s} S_i^z \;, \quad (1)$$

where S_i^z is the z component of spin operator $\vec{S}$ at site i, $J(>0)$ is an exchange coupling constant between nearest-neighboring spins, and the first summation runs over all nearest neighbor pairs. A positive value of J implies ferromagnetically coupled spins. $D(>0)$ is a single-ion magnetic anisotropy parameter determined by the spin-orbit coupling. A positive value of D indicates that the magnetic easy axis of an individual spin is along the $\pm z$ axis. Notice that our convention on D differs from other works. H is an external magnetic field applied to the spin system. We call the spin Hamiltonian Eq. (1) a $S \geq 1$ model. The eigenstates $|m\rangle$ of the spin Hamiltonian are

$$|m\rangle \;=\; |m_1\rangle \bigotimes |m_2\rangle \bigotimes \cdots \bigotimes |m_{N_s}\rangle \quad (2)$$

where $|m_i\rangle$ is the eigenstate of S_i^z and $m_i = -S, -S+1, ..., S-1, S$. For $S = 1$ and $D < 0$, the spin Hamiltonian Eq. (1) is known as the Blume-Capel model,[23,24] which was introduced to describe features of the phase diagram of He^3-He^4 mixtures as well as to understand a phase transition in UO_2. The $S \geq 1$ model can be applied to the following magnetic systems: arrays of weakly-interacting magnetic nanoparticles,[4,5] nanoscale single-molecule magnets such as Mn_{12} and Fe_8,[6,7,8] a $Mn(III)_2Ni(II)$ single-chain magnet,[10,11] and a Co ferrimagnetic compound.[9]

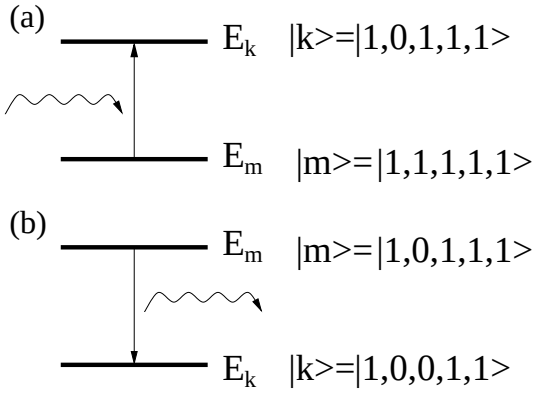

FIG. 1: Schematic diagram of (a) one-phonon absorption process for rotating the second spin from m_2 to $m_2 - 1$, and (b) one-phonon emission process for rotating the third spin from m_3 to $m_3 - 1$ for a five-spin $S = 1$ system. The wavy lines denote the phonons emitted or absorbed. (a) The energy difference $(E_k - E_m)$ equals $2J + D + H$ that is positive, and (b) $(E_k - E_m)$ equals $J + D + H$ that is negative when $-(2J + D) < H < -(J + D)$.

To understand spin relaxation in the $S \geq 1$ model, we assume that the spin system is weakly linearly coupled to a surrounding phonon bath in d dimensions. Since the phonon bath has much shorter relaxation time than the spin system, it is assumed that each spin is independently coupled to the bath. Then spin relaxation occurs through consecutive emission or absorption of a single phonon with energy that equals the cost of rotating a single spin from m_i to $m_i \pm 1$ in a single transition while keeping the rest of the spins fixed. Henceforth we call these rotations first-order one-phonon processes.

A phonon bath is described as a collection of simple harmonic oscillators so the phonon Hamiltonian is written as

$$\mathcal{H}_{\rm ph} \;=\; \sum_{\vec{q}} \hbar\omega_{\vec{q}} (c_{\vec{q}}^{\dagger} c_{\vec{q}} + \frac{1}{2}), \qquad \omega_{\vec{q}} = c\, q, \quad (3)$$

where $\vec{q}$ is the phonon wave vector, $\omega_{\vec{q}}$ is the angular frequency of a harmonic oscillator, $c_{\vec{q}}^{\dagger}$ and $c_{\vec{q}}$ are creation and annihilation operators of a phonon with wave vector $\vec{q}$, and c is the sound velocity in the lattice. The following spin-phonon coupling Hamiltonian $\mathcal{H}_{\rm sp-ph}$ has the simplest form that takes into account all possible first-order one-phonon processes.

$$\mathcal{H}_{\rm sp-ph} \;=\; \lambda \sum_{j=1}^{N} \sum_{\vec{q}} \sqrt{\frac{\hbar}{2NM\omega_{\vec{q}}}}\; q (S_j^+ c_{\vec{q}}^{\dagger} + S_j^+ c_{\vec{q}} + S_j^- c_{\vec{q}}^{\dagger} + S_j^- c_{\vec{q}}), \quad (4)$$

where λ is a coupling constant, N is the number of unit cells associated with the phonon bath, M is the mass of the particle in the unit cell, and $S_j^{\pm}$ are the raising

and lowering spin operators for site j. Here the polarization of the phonons is not considered for simplicity. The magneto-elastic coupling theory[25] suggests that the spin-phonon coupling must be proportional to a linear strain tensor, $\epsilon_{\alpha'\alpha} = \nabla_{\alpha'} u_\alpha$, where u_α is the α component of the displacement vector $\vec{u}$ and $\alpha', \alpha \in \{x, y, z\}$. The displacement vector can be expressed in terms of $c^\dagger_{\vec{q}}$ and $c_{\vec{q}}$, and a Fourier transform is carried out on $\epsilon_{\alpha'\alpha}$. This explains the dependence of the prefactor of $\mathcal{H}_{\rm sp-ph}$ on the wave vector $\vec{q}$. Equation (4) contains the minimum number of terms required to rotate the spin vectors via one-phonon emission or absorption processes. Notice that the spin system includes a nearest-neighbor exchange interaction, in contrast to works reported by other groups[7,8]. Due to the exchange interaction, a transition from m_l to $m_l - 1$ does not uniquely determine the sign of the energy difference $E_k - E_m$ between the two states. For example, when $m_l = 1$, $E_k - E_m$ is positive for Fig. 1(a), while $E_k - E_m$ is negative for Fig. 1(b). The same rule is applied to transition from m_l to $m_l + 1$.

Using Fermi's golden rule, within perturbation theory, we calculate the transition rate from state $|m\rangle = |m_1\rangle \bigotimes |m_2\rangle \bigotimes \cdots \bigotimes |m_l\rangle \bigotimes \cdots \bigotimes |m_N\rangle$ to state $|k\rangle = |m_1\rangle \bigotimes |m_2\rangle \bigotimes \cdots \bigotimes |m'_l\rangle \bigotimes \cdots \bigotimes |m_N\rangle$, where $m'_l = m_l \pm 1$. States $|m\rangle$ and $|k\rangle$ differ by the rotation of a single spin ($m_l \rightarrow m_l \pm 1$) at site l. We first consider the transition rate W_{km} from $|m\rangle$ to $|k\rangle$ for emission of one phonon with energy $\hbar\omega_{\vec{q}}$, as illustrated in Fig. 1(b).

$$W_{km} = \frac{2\pi}{\hbar} \sum_{n_{\vec{q}}} \sum_{\vec{q}} |\langle n_{\vec{q}} + 1, k|\mathcal{H}_{\rm sp-ph}|n_{\vec{q}}, m\rangle|^2 \, \rho_{\rm ph} \, \delta(\hbar\omega_{\vec{q}} - (E_m - E_k)), \quad (5)$$

$$= \frac{2\pi}{\hbar} \sum_{n_{\vec{q}}} \sum_{\vec{q}} \frac{\lambda^2 \, \hbar}{2NM\omega_{\vec{q}}} \, q^2 (n_{\vec{q}} + 1)\rho_{\rm ph} |\langle k|(S^+_l + S^-_l)|m\rangle|^2 \delta(\hbar\omega_{\vec{q}} - (E_m - E_k)) \quad (6)$$

where $\rho_{\rm ph}$ is the phonon density of states, $n_{\vec{q}}$ is the eigenvalue of the phonon number operator, and $c^\dagger_{\vec{q}}|n_{\vec{q}}\rangle = \sqrt{n_{\vec{q}} + 1}|n_{\vec{q}}+1\rangle$ is used. Here E_k and E_m are the energies of states $|k\rangle$ and $|m\rangle$ calculated from the spin Hamiltonian, Eq. (1), and the energy difference ΔE is given by

$$\Delta E(m_l \rightarrow m_l \pm 1) \equiv E_k - E_m = \mp J \sum_{k \in nn(l)} m^{(l)}_k \mp D(2m_l \pm 1) \quad (7)$$

where the sum runs over nearest neighbors of site l. Using the Bose-Einstein distribution function, one knows that

$$\sum_{n_{\vec{q}}} (n_{\vec{q}} + 1)\rho_{\rm ph} = \frac{1}{1 - e^{-\beta\hbar\omega_{\vec{q}}}} \quad (8)$$

where k_B is the Boltzmann constant, T is the temperature, and $\beta = 1/(k_B T)$. Assuming that the bath relaxes much faster than the spin system, we integrate over all degrees of freedom of the bath and convert $\sum_{\vec{q}}$ into $[(Na^d)/(2\pi)^d] \int d^d q$, where a is the lattice spacing. Then the transition rate from state $|m\rangle$ to $|k\rangle$ becomes

$$W_{km} = \frac{\lambda^2 \, \tilde{N}}{\gamma\eta\hbar^{d+1}c^{d+2}} \, \frac{(E_m - E_k)^d}{1 - e^{-\beta(E_m - E_k)}}, \quad E_m - E_k > 0 \quad (9)$$

$$\tilde{N} = (S + m_l)(S - m_l + 1)\delta_{k_l, m_l - 1} + (S - m_l)(S + m_l + 1)\delta_{k_l, m_l + 1}, \quad (10)$$

$$\gamma = 2\pi \ (d = 3), \quad 2 \ (d = 1, 2), \quad (11)$$

where η is a mass density associated with the bath and k_l is the quantum number of the lth spin for state $|k\rangle$. The transition rate for absorption analogously becomes

$$W_{km} = \frac{\lambda^2 \, \tilde{N}}{\gamma\eta\hbar^{d+1}c^{d+2}} \, \frac{(E_k - E_m)^d}{e^{\beta(E_k - E_m)} - 1}, \quad E_k - E_m > 0 \quad (12)$$

Henceforth, we refer to the derived transition rates, Eqs. (9) and (12), as phonon-assisted transition rates.

III. CONSEQUENCES OF PHONON-ASSISTED TRANSITION RATES

The derived phonon-assisted transition rates are generalized forms of those for the Ising model discussed in Refs.13,14,15. According to Eqs. (9) and (12), the transition rates are highest for $m_l = 0$ and lowest for $m_l = \pm S$ for large S. A transition rate[8] similar to the derived rates was obtained for an *isolated* spin cluster embedded in a lattice instead of interacting spin clusters. In this formalism, the single-ion anisotropy parameter D corresponds to the coupling constant λ in Eq. (4). Assuming that $\lambda \sim D$, we estimate the magnitude of the prefactor of the $d = 3$ phonon-assisted transition rates, Eqs. (9) and (12), for example, for the nanoscale single-molecule magnet Mn_{12}. Using measured parameter values such as $S = 10$, $m_l = 10$, $J = 0.01$ K, $\eta = 1.83 \times 10^3$ kg/m^2 [Ref.26], and $c = 1.45 \times 10^3$ m/s,[7] we find the prefactor to be 0.00041 s^{-1}. Here we use $J = 0.01$ K due to the large intermolecular separation in this system, although it was not directly measured. To associate the derived transition rates with magnetization relaxation times for various nanoscale systems, one needs to solve a master equation including the derived transition rates or perform kinetic

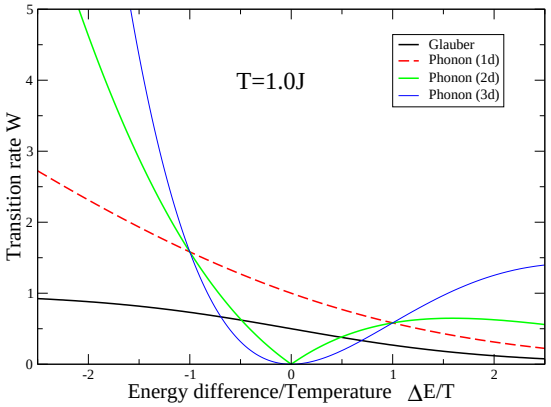

FIG. 2: Transition rates W vs $\Delta E/T$ for the Glauber and phonon-assisted transition rates in the case of $d = 1, 2,$ and 3 dimensional phonon baths, computed at temperature $T = 1.0J/k_B$. The prefactor of the phonon-assisted transition rates was not included.

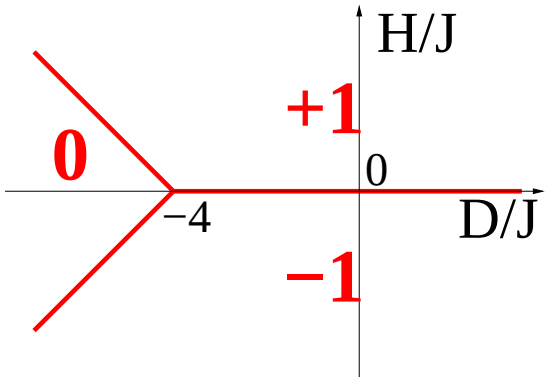

FIG. 3: Phase diagram of the Blume-Capel model with $D > 0$ in the spin Hamiltonian (1) at zero temperature.[27] The equilibrium spin configurations are shown in the three different regions.

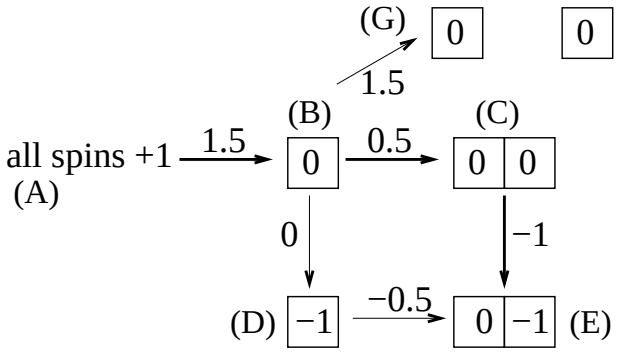

FIG. 4: Schematic diagram of relaxation of magnetization for a ferromagnetic $S = 1$ Blume-Capel model at $H = -3.25J$ and $D = 0.75J$, via first-order one-phonon processes, $m_l \to m_l \pm 1$. State (A) denotes all spins aligned along the $+z$ axis, and state (B) a single $m_l = 0$ spin in the sea of $m_i = +1$ spins. The boxes represent rotated spins from the $+z$ axis in the initial state. State (C) represents two nearest-neighbor $m_l = 0$ spins in the sea of $m_i = +1$ spins, while state (G) represents two $m_l = 0$ spins that are not nearest neighbors. The numbers next to the arrows indicate the energy difference ΔE defined by Eq. (7). With the $d = 2$ phonon-assisted transition rates, the spin system relaxes through (A)→(B)→(C)→(E) rather than (A)→(B)→(D)→(E). The thick arrows represent the most probable path for relaxation with the phonon-assisted rates. The thin arrows denote the most probable path with the Glauber transition rate.

Monte Carlo simulations with the rates. Hereafter we focus on the latter approach.

In Fig. 2 the phonon-assisted transition rates for $d = 1, 2,$ and 3 dimensional phonon baths are shown as functions of $\Delta E/T$ at temperature $T = 1.0J$ and compared to the Glauber transition rate, $1/(e^{\beta(E_k - E_m)} + 1)$. The main difference between the phonon-assisted and Glauber transition rates originates from the nature of the bath coupled to the spin system. When degenerate states are involved in transitions, this difference becomes prominent. In the $d = 2$ and 3 phonon-assisted transition rates, transitions between degenerate states are forbidden because $W_{km} = 0$ when $\Delta E = 0$. In the case of $d = 1$, the rate does not vanish for $\Delta E = 0$, but rather decreases monotonously with $\Delta E/T$ like the Glauber transition rate. Ramifications of the forbidden transitions on dynamic and equilibrium properties are discussed in Monte Carlo simulations. For simplicity, we consider a ferromagnetic $S = 1$ model [the Blume-Capel model with $D > 0$ in the spin Hamiltonian, Eq. (1)] on a $L \times L$ square lattice with the $d = 2$ phonon-assisted transition rates unless specified otherwise.

A. Dynamic properties

We investigate the effects of the forbidden transitions on the lifetime of the metastable state for the $S = 1$ Blume-Capel model below the critical temperature. The equilibrium spin configurations for the model are shown in different regions in Fig.3.[27] The nucleation and metastability for the model were studied for $-4J < D < -3J$ and $-J < H < -(4J + D)$ in Ref.27. The critical temperature T_c increases as D/J increases at H=0. The value of T_c at $D = 0$ was calculated using different methods. Bethe-lattice approximation gave rise to $2.065J/k_B$[28] and the effective field theory suggested $1.952J/k_B$.[29] Expanded Bethe-Peierls approximation produced $1.915J/k_B$,[30] and Monte Carlo simulations suggested that the critical temperature at H=0 is $1.6950J/k_B$ at $D = 0$ and $2.1855J/k_B$ at $D = 5J$.[31] Suppose that all spins are initially aligned along the $+z$ axis. When an external magnetic field is applied along the $-z$ axis, the initial state becomes metastable. When $-(4J + D) < H < 0$, at low temperatures, the spin system relaxes toward the stable state (all spins along the $-z$ axis) via creating a single critical droplet consisting of connected $m_i = -1$ spins. (In the regime studied in Ref.27 multiple critical droplets are formed.) To give a

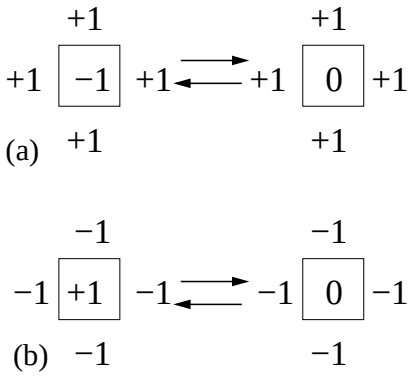

FIG. 5: Transitions forbidden by first-order one-phonon processes for a $S = 1$ spin system on a square $L \times L$ lattice with $D = 4J$ and $H = 0$ in which $W_{km} = 0$. (a) Initial state of -1 with nearest neighbors of $+1$. (b) Initial state of $+1$ with nearest neighbors of -1.

specific example, we consider $H = -3.25J$, $D = 0.75J$, and $T < 0.02J/k_B$. Figure 4 illustrates a few possible relaxation paths from the metastable state. The initial state (A) can first relax to state (B), which represents a single $m_l = 0$ spin in the sea of $m_l = +1$ spins. Then state (B) can relax to one of the states (C), (D), or (G), where state (C) denotes a single $m_l = -1$ spin in the sea of $m_l = +1$ spins and state (D) [state (G)] two nearest-neighbor $m_l = 0$ spins [two $m_l = 0$ spins that are not nearest neighbors] in the sea of $m_l = +1$ spins. Transitions between states (B) and (D) are forbidden because $\Delta E = \pm(4J - D + H) = 0$. Thus, the system can relax from state (B) to either state (C) or (G). The most likely path among the alternative ones is (B)→(C)→(E), as indicated by the thick arrows in Fig. 4. Thus, for the $d = 2$ phonon-assisted transition rate, the critical droplet is state (C). As a result, the energy barrier to be overcome in order to reach the stable state, is $2.0J$, while it is $1.5J$ for the Glauber transition rate. Accordingly, the relaxation time becomes longer than that for the Glauber transition rate. In an Ising system coupled to a phonon bath, a similar behavior has been found at $H = -2J$.[13,14,15] If there are no alternative paths, the relaxation time diverges. For a two-electron state in a quantum dot, the measured spin-lattice relaxation time was observed to diverge at a particular magnetic field where the triplet and the singlet states became degenerate.[3]

B. Equilibrium properties

The $d = 1, 2$, and 3 phonon-assisted transition rates satisfy detailed balance. Thus, equilibrium properties obtained using the derived transition rates must agree with those obtained using different transition rates in Monte Carlo simulations. However, there is a caveat in this statement because of forbidden transitions between degenerate states for the $d = 2$ and 3 phonon-assisted rates. In some cases the forbidden transitions would prevent the spin system from relaxing to the equilibrium state if we start with a particular initial state. As an example, we consider $D = 4J$ and $H = 0$. As illustrated in Fig. 5, transitions between $m_l = +1$ ($m_l = -1$) and $m_l = 0$ with the sum of the nearest neighbors fixed as -4 ($+4$) are not allowed because $\Delta E = -4J \pm H + D = 0$. So if we started with a checkerboard initial state as shown in Fig. 6 in Monte Carlo simulations, the system would stay indefinitely at the initial state because $W_{km} = 0$ for any possible single-spin rotations. However, we have confirmed that the system reaches equilibrium if we start with a random initial state or a state slightly modified from the checkerboard pattern. (Even one defect site in the perfect checkerboard state is sufficient.) A similar feature was reported in the time evolution of field-driven solid-on-solid interfaces using the $d = 2$ phonon-assisted transition rate.[22]

Monte Carlo simulations were performed for $D = 4J$ and $H = 0$ with periodic boundary conditions and a ran-

+1	−1	+1	−1	+1	−1
−1	+1	−1	+1	−1	+1
+1	−1	+1	−1	+1	−1
−1	+1	−1	+1	−1	+1
+1	−1	+1	−1	+1	−1
−1	+1	−1	+1	−1	+1

FIG. 6: A checkerboard state for a $S = 1$ spin system on a

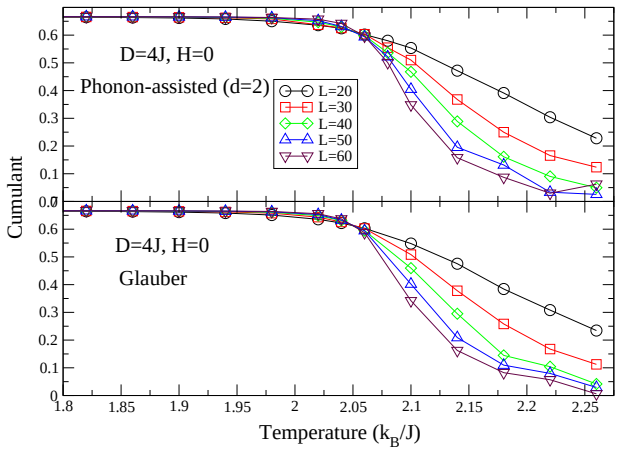

FIG. 7: Cumulant U_L [Eq. (13)] vs temperature calculated from Monte Carlo simulations using (top) the Glauber and (bottom) the $d = 2$ phonon-assisted transition rates for $S = 1$ spins on a $L \times L$ square lattice at $D = 4J$ and $H = 0$. Random initial states and periodic boundary conditions were used. For the fixed point of the cumulant and critical temperature, see the text.

dom initial state. $L = 20, 30, 40, 50$, and 60 were considered at several different temperatures. The average absolute magnetization per site $\langle|m|\rangle$ and cumulant U_L were calculated.

$$\langle|m|\rangle = \frac{1}{\tilde{M}}\sum_{i=1}^{\tilde{M}}\frac{1}{L^2}\left|\sum_{j=1}^{L^2}S_j^{(i)}\right|, \quad U_L = 1 - \frac{\langle m^4\rangle}{3\langle m^2\rangle^2} \quad (13)$$

where m is the magnetization per site and $\tilde{M}$ is the total number of Monte Carlo steps. It was found that $\langle|m|\rangle$ (not shown) and U_L (Fig. 7) as functions of temperature agree with those obtained using the Glauber transition rate for the different system sizes. For the Glauber transition rate, the values of U_L for the different system sizes intersect with one another at $U_L^\star$=0.611± 0.008 and T_c=2.052±0.005 J/k_B, while for the phonon-assisted transition rate we have $U_L^\star$=0.611± 0.009 and T_c=2.052±0.006 J/k_B. So both transition rates give rise to the same critical temperature. This critical temperature is slightly lower than that reported in Ref.31, $2.13J/k_B$.

IV. HIGHER-ORDER PROCESSES

We have, so far, discussed spin relaxation caused by first-order one-phonon processes, $m_l \to m_l \pm 1$. However, higher-order processes such as multi-phonon processes and second-order one-phonon processes ($m_l \to m_l \pm 2$), can also contribute to the spin relaxation. Their contributions become significant especially when encountering transitions forbidden by the first-order one-phonon processes. In this case, the spin system would find less costly paths via the higher-order processes than paths directed by the first-order processes. Thus, the relaxation time becomes shortened and the system may recover the same relaxation time or energy barrier as the Glauber transition rate. The system starting with the checkerboard state (Fig. 6) can be also relaxed to equilibrium.

Recently, multi-phonon processes such as Raman processes and two-phonon processes were considered in a spin-phonon relaxation rate for rigid atomic clusters, and it was shown that there are no closed analytical forms for the rate.[32] In the current study, we focus on second-order one-phonon processes as higher-order processes. These second-order processes were included as a part of the relaxation mechanism for the single-molecule magnet Mn_{12}.[7] The simplest form of the spin-phonon coupling Hamiltonian for these processes is given by

$$\mathcal{H}_{\rm sp-ph}^{(2{\rm nd})} = \lambda'\sum_{j=1}^{N}\sum_{\vec{q}}\sqrt{\frac{\hbar}{2NM\omega_{\vec{q}}}}\, q[(S_j^+)^2 c_{\vec{q}}^\dagger + (S_j^-)^2 c_{\vec{q}}^\dagger + (S_j^+)^2 c_{\vec{q}} + (S_j^-)^2 c_{\vec{q}}], \quad (14)$$

where λ' is a coupling constant and $|\lambda'| \ll |\lambda|$. Following the method used in Sec. II, we obtain the transition rate

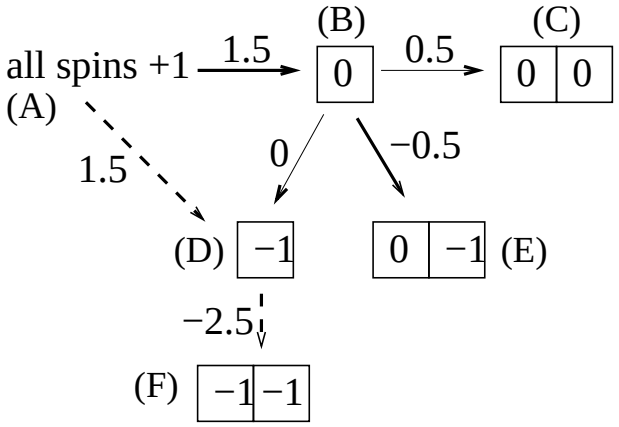

FIG. 8: Schematic diagram of relaxation of magnetization for a $S = 1$ spin system at $H = -3.25J$ and $D = 0.75J$ when both first-order ($m_l \to m_l \pm 1$) and second-order one-phonon processes ($m_l \to m_l \pm 2$) are considered. The thick solid and dashed arrows represent two highly probable paths for relaxation. Compared to Fig. 4, the spin system can relax from state (A) to state (E) through (B), or to state (F) through (D). The numbers next to the arrows indicate the energy difference ΔE defined by Eqs. (7) and (17).

$W_{km}^{(2{\rm nd})}$ from state $|m\rangle$ to $|k\rangle$, where these two states differ by a single spin rotation at site l, $m_l' = m_l \pm 2$.

$$W_{km}^{(2{\rm nd})} = \frac{(\lambda')^2\, N'}{\gamma\eta\hbar^{d+1}c^{d+2}}\left|\frac{(E_k - E_m)^d}{e^{\beta(E_k-E_m)}-1}\right|, \quad (15)$$

$$N' = (S+m_l)(S-m_l+1)(S+m_l-1)(S-m_l+2)\delta_{k_l,m_l-2} + (S-m_l)(S+m_l+1)(S-m_l-1)(S+m_l+2)\delta_{k_l,m_l+2} \quad (16)$$

where γ is defined in Eq. (11). The energy difference $E_k - E_m = \Delta E$ is

$$\Delta E(m_l \to m_l \pm 2) = \mp 2J\sum_{k\in nn(l)} m_k^{(l)} \mp 4D(m_l \pm 1) \mp 2H, \quad (17)$$

where the sum runs over nearest neighbors of site l. This formula is applied to both emission and absorption processes.

When the second-order transition rate $W_{km}^{(2{\rm nd})}$ is included in the calculation of the lifetime of the metastable state, relaxation scenarios are greatly modified as illustrated in Fig. 8. With the same parameter values used in Sec.III.A ($D = 0.75J$ and $H = -3.25J$), the system can now relax through transitions as indicated by the thick dashed arrows [(A)→(D)→(F)] or by the thick solid arrows [(A)→(B)→(E)] in Fig. 8. None of these transitions involve degenerate states. The critical droplet for the first relaxation route is state (D), while that for the second route is state (B). In both relaxation paths, the energy barrier is $1.5J$, which is the same as that for the Glauber transition rate. In the case of equilibrium Monte

Carlo simulations, the second-order processes allow the system to relax via alternative second-order transitions with lower energy cost but $\Delta E \neq 0$. So the checkerboard initial state (Fig. 6) can reach equilibrium for $D = 4J$ and $H = 0$. It is confirmed that for $L = 20$ the equilibrium properties computed with addition of $W_{km}^{(2\mathrm{nd})}$ to W_{km} agree with those obtained using the Glauber transition rate.

V. CONCLUSION

We have considered the $S \geq 1$ model weakly coupled to a one-, two-, or three-dimensional phonon bath and derived corresponding transition rates from the spin-phonon coupling Hamiltonian. The derived phonon-assisted transition rates for two- and three- dimensional baths differ from other transition rates in that the former rates become zero for degenerate states. This caused some transitions to be forbidden by the first-order one-phonon assisted transition rates, increasing the magnetization relaxation time. Using a combination of the first-order one-phonon processes with the second-order processes, however, the system found more energy-efficient paths to equilibrium, and the relaxation time shortened. These results represent a major step toward developing physically realistic kinetic Monte Carlo simulations for magnetic spin systems.

Acknowledgments

The author is grateful to M. A. Novotny, L. Solomon, and P. A. Rikvold for discussions.

* Electronic address: kyungwha@vt.edu

[1] W. Zhang, V. V. Dobrovitsky, K. A. Al-Hassaniah, E. Dogotto and B. N. Harmon Phys. Rev. B **74**, 205313 (2006).
[2] N. V. Prokof'ev and P.C.E. Stamp, Rep. Prog. Phys.**63**, 669 (2000).
[3] T. Meunier, I. T. Vink, L. H. Willems van Beveren, K.-J. Tielrooij, R. Hanson, F. H. L. Koopens, H. P. Tranitz, W. Wegscheider, L. P. Kouwenhoven, and L. M. K. Vandersypen, Phys. Rev. Lett. **98**, 126601 (2007).
[4] P. Zhang, F. Zuo, F.K. Urban, A. Khabari, P. Griffiths, A. Hosseini-Tehrani, J. Mag. Mag. Mat. **225**, 337 (2001).
[5] Y.I. Kim, D. Kim, C.S. Lee, Physica B-Cond. Matt. **337**, 42 (2003).
[6] P. Politi, A. Rettori, F. Hartmann-Boutron, and J. Villain, Phys. Rev. Lett. **75**, 537 (1995)
[7] M. N. Leuenberger and D. Loss, Phys. Rev. **61**, 1286 (2000).
[8] E. M. Chudnovsky, D. A. Garanin, and R. Schilling, Phys. Rev. B **72**, 094426 (2005).
[9] A. Caneschi, D. Gatteschi, N. Lalioti, R. Sessoli, L. Sorace, V. Tangoulis, and A. Vindigni, Chem-Eur. J. **8**, 286 (2002).
[10] C. Coulon, R. Clérac, L. Lecren, W. Wernsdorfer, and H. Miyasaka, Phys. Rev. B **69**, 132408 (2004).
[11] J. Kishine, T. Watanabe, H. Deguchi, M. Mito, T. Sakai, T. Tajiri, M. Yamashita, and H. Miyasaka, Phys. Rev. B **74**, 224419 (2006).
[12] L. Solomon, M.A. Novotny, S. Caliskan, K. Park, and P.A. Rikvold, submitted to Phys. Rev. B.
[13] M. A. Novotny and K. Park, Computer Phys. Commun. **147**, 737 (2002).
[14] K. Park and M. A. Novotny, in *Computer Simulations Studies in Condensed Matter Physics XIV*, edited by D.P. Landau, D. Lewis, and H.-B. Schüttler, (Springer-Verlag, Berlin, 2002), p. 182.
[15] K. Park, M. A. Novotny, and P. A. Rikvold, Phys. Rev. E **66**, 056101 (2002).
[16] R. J. Glauber, J. Math. Phys. **4**, 294 (1963).
[17] N. Metropolis, A. Rosenbluth, M. Rosenbluth, A. Teller, and E. Teller, J. Chem. Phys. **21**, 1087 (1953).
[18] P.-A. Martin, J. Stat. Phys. **16**, 149 (1977).
[19] P. A. Rikvold and M. Kolesik, J. Phys. A: Math. Gen. **35**, L117 (2002).
[20] K. Park, P. A. Rikvold, G. M. Buendía, and M. A. Novotny, Phys. Rev. Lett. **92**, 015701 (2004).
[21] K. Saito, S. Takesue, and S. Miyashita, Phys. Rev. E **61**, 2397 (2000).
[22] G. M. Buendía, P. A. Rikvold, M. Kolesik, K. Park, and M. A. Novotny, Phys. Rev. B **76**, 045422 (2007).
[23] H.W. Capel, Physica **32**, 966 (1966).
[24] M. Blume, Phys. Rev. **141**, 517 (1966).
[25] E. Callen amd H. B. Callen, Phys. Rev. **139**, A455 (1965).
[26] T. Lis, Acta Crystallogr. B **36**, 2042 (1980).
[27] E.N.M. Cirillo and E. Olivieri, J. Stat. Phys. **83**, 473 (1996).
[28] Y. Tanaka and N. Uryû, J. Phys. Soc. Japan **50**, 1140 (1981).
[29] H. Polat, Ü. Akinci, and Í. Sökmen, Phys. Stat. Sol. B **240**, 189 (2003).
[30] A. Du, Y.Q. Yü, and H.J. Liu, Physica A **320**, 387 (2003).
[31] R. da Silva, N. A. Alves, and J.R. Drugowich de Felício, Phys. Rev. E **66**, 026130 (2002).
[32] C. Calero, E. M. Chudnovsky, and D. A. Garanin, Phys. Rev. B **74**, 094428 (2006).